Highly accurate simulations and benchmarking of molecule-surface reactions

Tchakoua, T.

2

Chapter 2

Towards a Specific Reaction Parameter Density Functional for H_2 + Ni(111): Comparison of Theory with Molecular Beam Sticking Experiments

This Chapter is based on:

Tchakoua, T; Smeets, E. W.; Somers, M.; Kroes, G. J. Toward a Specific Reaction Parameter Density Functional for H_2+ Ni(111): Comparison of Theory with Molecular Beam Sticking Experiments. *J. Phys. Chem. C* **2019**, *123*, 20420–20433

Abstract

Accurate barriers for rate controlling elementary surface reactions are key to understanding, controlling and predicting the rate of overall heterogeneously catalyzed processes. The specific reaction parameter approach to density functional theory (SRP-DFT) in principle allows chemically accurate barrier heights to be obtained for molecules dissociating on metal surfaces, and such accurate barriers are now available for four H_2-metal and three CH_4-metal systems. Also, there is some evidence that SRP density functionals (SRP-DFs) may be transferable among systems in which the same molecule interacts with a low index face of metals belonging to the same group. To extend the SRP database, here we take a first step to obtain an SRP-DF for H_2 + Ni(111), by comparing sticking probabilities (S_0) computed with the quasi-classical trajectory method with S_0 measured in several molecular beam experiments, using potential energy surfaces computed with several density functionals. We find that the SRP-DF for H_2 + Pt(111) is not transferable to H_2 + Ni(111). On the other hand, the PBE-vdW2 functional describes the molecular beam experiments on H_2 + Ni(111) we deem to be most accurate with chemical accuracy, and may therefore be considered a candidate SRP-DF for this system, of which the quality still

needs to be confirmed through comparison with an experiment it was not fitted to. However, the different molecular beam sticking measurements we considered showed discrepancies with one another and with the theory for incidence energies > 0.2 eV, and it would be good if better defined and more accurate experiments would be done for these energies to resolve these differences.

2.1 Introduction

The dissociative chemisorption (DC) of a molecule on a metal surface is often the rate-controlling step of a heterogeneously catalyzed process, famous examples of such processes being steam reforming[1] and ammonia production[2]. These processes are important to industrial companies[3](e.g., the steam reforming reaction is used for the commercial production of the hydrogen[1]) and improving the efficiency of heterogeneously catalyzed processes is of huge importance.

To understand how heterogeneous catalysis works from a quantitative point of view, being able to accurately model DC is important. For this, it is relevant to have an accurate potential energy surface (PES) with accurate barrier heights available. Experimentally, it is not possible to measure the barrier height for DC. The observable usually measured experimentally is the sticking probability S_0. Therefore, the only way to assess a computed barrier height and PES is through a theoretical approach in which a PES is used in dynamics calculations to calculate S_0 as a function of average incidence energy and comparison with experiment for this and other observables[4,5]. Only when experimental data are reproduced to a sufficiently large extent can a claim be made that the computed barrier is of high accuracy, with chemical accuracy defined as accurate to within 1 kcal/mol[4–6].

Unfortunately, *ab initio* or non-empirical electronic structure methods that can compute molecule-metal surface interaction energies to within chemical accuracy are not yet available (see also Refs.[6] and[7], and **Chapter 3**). Presently, the most efficient electronic structure method that can be used to map out the PES of the interaction of the molecule with metal surface is density functional theory (DFT) using an approximate exchange-correlation (XC) functional, which is usually taken at the generalized gradient approximation (GGA) level[8–10]. With the best GGA functional for barrier heights (MOHLYP) the mean unsigned error (MUE) for a database of gas phase barrier heights is 3.8 kcal/mol[11]. Even with the highest level semi-local functionals chemical accuracy has not been achieved yet for such reactions, the best result (MUE=1.8 kcal/mol) having been obtained with a functional at the meta non-separable gradient approximation level[12]. From the benchmark study we will present in **Chapter 3**, the PBE

GGA functional performs best on the SBH17 database for DC on metal surfaces, with a MAE of 2.4 kcal/mol.

To overcome this problem of DFT accuracy, Díaz et al.[4] proposed an implementation of specific reaction parameter (SRP) DFT (SRP-DFT). In this approach the exchange-correlation functional is fitted with one adjustable parameter to a set of experimental data for a molecule reacting on the surface that is particular sensitive to the reaction barrier height. Ideally, the quality of the SRP functional is tested by checking that it can also be used to reproduce other experiments on the same system, to which it was not fitted[4,5]. With this SRP approach, one might say we have now obtained a small database of chemically accurate barriers for molecules reacting on metal surfaces, as discussed in **Chapter 3**.

In some cases, transferability of an SRP density functional (SRP-DF) among similar systems has been established. In the study of Migliorini et al.[13], it has been shown that the SRP-DF for CH_4+Ni(111) could also be used to obtain chemical accuracy for CH_4+Pt(111). This suggests that an SRP-DF for a specific molecule interacting with a low index face of a specific metal might also be an SRP-DF for the same molecule reacting on a low index face of a metal belonging to the same group. However, this type of transferability was found not to hold when the SRP-DF for H_2+Cu(111) was tested for D_2+Ag(111)[14], for which chemical accuracy was not obtained. Clearly more tests are needed on to what extent SRP-DFs might be transferable among similar systems, and how the SRP-DFs should be designed to achieve maximum transferability.

Given the number of the above systems for which the SRP functional could be fitted to reproduce the experimental results, there is no a doubt that the approach can be effective. However, this effort is still at an early stage, and more efforts are needed to extend the database. Being semi-empirical and in need of validation, the SRP-DFT approach is not without problems. One important problem for some systems concerns the availability of accurate and well-defined experiments (see H_2+Pd(111)[15] and H_2+Pt(111)[16]). Obviously, the semi-empirical SRP-DFT approach is no more accurate than the underlying experimental data. This problem can become severe if different sets of measurements of the sticking probability for a specific system show widely differing results[15].

H_2 DC on a metal surface may be considered as a benchmark system for electronic structure and surface science reaction dynamics methods[17–20], for several reasons. First of all, hydrogen is a small and simple molecule just containing two electrons. If the surface degrees of freedom are neglected, the PES of the H_2 reacting on this surface depends on only six degrees of freedom (six-dimensional, 6D), and can be mapped out easily. In principle, also the degrees of freedom of the surface atoms should be taken in to account (the

surface phonons) and electron-hole (e-h) pair excitation[6,18,21,22]. However, for H_2 dissociation on metal surfaces, the approximation of keeping the surface static with the metal atoms in their ideal lattice position (neglecting surface phonons) has been proven to work well for activated sticking on cold surfaces (surface temperature not larger than room temperature)[20]. Likewise, it is usually a good approximation to neglect electron-hole (e-h) pair excitation[20], as also shown in very recent work[23,24]. Finally, a large amount of experimental data is available for reaction of H_2 on metal surfaces[20].

H_2+Ni(111) has been the subject of many investigations, theoretically as well as experimentally. Steinrück et al.[25] performed molecular beam experiments on the sticking using Maxwellian beams of hydrogen, predicting a linear dependence of the sticking probability upon mean incidence energy in the range 1.7-15 kJ.mol^{-1} (see Fig. 2.1). In contrast, Robota et al.[26] in the same year (1985) predicted a parabolic dependence of the sticking probability upon mean energy in the range of 1.0-11.6 kJ.mol^{-1} using nozzle beams (i.e supersonic) of H_2 and D_2 (see Fig. 2.1). Hayward and Taylor[27] also used nozzle beams, of H_2 and D_2 with collision energies in the range of 1.0-9.2 kJ.mol^{-1}, and found a linear dependence of the sticking coefficient of H_2 on Ni(111) upon energy, as Steinrück et al. did (Fig. 2.1). They concluded that there was probably a problem with the experiments of Robota et al., which did not yield a linear dependence.

In 1989, Rendulic et al.[28] reported new experimental data on H_2 + Ni(111), extending the incidence energy range to higher energies, i.e., to almost 0.4 eV. They also used supersonic beams and found a linear dependence of the sticking coefficient upon mean energy in the conflicting region of Robota et al. and Hayward and Taylor (Fig. 2.1). At lower incidence energies, the S_0 of Rendulic et al. were in good agreement with those of Hayward and Taylor. Somewhat later, Resch et al. (from the group of Winkler and Rendulic) revisited the H_2/Ni(111) system with supersonic molecular beam experiments[29], focusing on the effect of co-adsorbed inhibitors and promotors (potassium and oxygen). They found that potassium on Ni(111) acts as an inhibitor to the dissociation of hydrogen (Fig. 2.1). The clean surface S_0 of Resch et al. agree well with those of Rendulic et al. for E_i up to 0.2 eV, but exceed the values of Rendulic et al. for larger E_i (Fig. 2.1). This discrepancy, which was not addressed by Resch et al., may indicate some uncertainty in the supersonic molecular beam data for $E_i > 0.2$ eV. Most recently, new experimental data for H_2+Ni(111) were reported by Christine Hahn of the Juurlink/Kleyn group, in her Ph.D thesis[30]. Their observed S_0 are somewhat larger than those of Rendulic et al. and Resch et al., which may be related to the data having been taken for a circular crystal so that more reactive stepped surfaces are also sampled and to the data not having been presented as a function of the average beam energy.

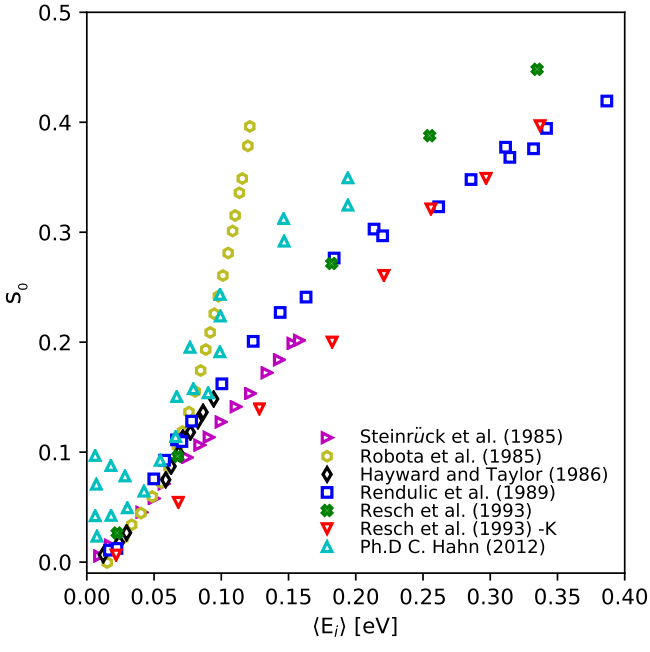

FIGURE 2.1: Comparison of the energy dependence of the sticking probability of H_2 on Ni(111) for seven different sets of experimental data: Steinrück et al.[25](magenta left triangle), Robota et al.[26](olive hexagon), Hayward and Taylor[27](black rhombus), Rendulic et al.[28](blue square), Resch et al.[29](green cross) using a clean surface of Ni(111)(Zero-coverage), Resch et al.[29](red down triangle) using an inhibitor (Ni(111) surface coverage by potassium) and C. Hahn Ph.D thesis[30](cyan upper triangle).

A common point of the experimental data is that extrapolation to lower incidence energies yields a negative intercept, which indicates that the dissociation is slightly activated, with a positive minimum barrier height. Three experiments show similar results for the low energy range, i.e., those of Rendulic et al.[28], Resch et al.[29] and Hayward and Taylor[27]. For this study, we will focus on the Rendulic et al.[28] experiments, which also give results for high energies, but we will also compare our computational results to those of Resch et al..

To understand the experiments discussed, several theoretical studies have been carried out. Unfortunately, most of these studies suffer from the use of a somewhat inaccurate PES. This may have been due to the use of an approximate fit expression (e.g., a London -Eyring -Polanyi -Sato form)[31] or to the use of

a standard GGA functional[32]. Kresse[32] used a non-empirical GGA functional to obtain a PES for H_2+Ni(111), employing the PW91 functional[33,34]. The classical trajectory method was used to compute the sticking coefficient, with the vibrations and rotations of H_2 described by an ideal gas at the temperature of the nozzle used in the experiments. His theoretical data for the DC of H_2 at specific incidence energy was compared to the molecular beam data of Rendulic et al.. Kresse obtained qualitative agreement, but quantitative agreement was not yet obtained. Specifically, Kresse found that the reaction was activated, but the reaction probability was overestimated. He concluded that at least part of the difference might have been due to the use of the classical trajectory method he used not taking into account zero-point energy effects appropriately. He suggested that improved agreement with experiment might be obtainable with a quantum dynamical method.

In the present work, we attempt to derive a SRP-DF for H_2+Ni(111). We first test the transferability of the previously fitted SRP functional for H_2+Pt(111)[35] to H_2+Ni(111). However, we also use other functionals to generate the PES, where DFs are tested that are semi-local (GGA) and that are non-local (GGA for exchange and vdW-DF1[36] or vdW-DF2[37] for correlation). We also evaluate the sensitivity of the computed sticking probabilities to the molecular beam parameters that are employed to simulate the experiment. Additionally, we investigate the accuracy of the dynamics method we use for the simulation of molecular beam sticking probabilities (i.e., the quasi-classical trajectory (QCT) method) by comparing with quantum dynamics (QD) results for a few selected initial rovibrational states.

Our **Chapter** is organized as follows: First, we describe the theoretical methods used in this work in Section 2.2. Section 2.2.1 describes the dynamical model and Section 2.2.2 describes the construction of the PES. The CRP interpolation method is described in Section 2.2.3. The dynamics methods that are used here to study H_2+Ni(111) are explained in Section 2.2.4. Section 2.2.5 describes how we calculate the observables. In Section 2.3, the results of the calculations are shown and discussed. Section 2.3.1 describes the computed PESs, and Sections 2.3.2 and 2.3.3 provide discussion on the comparison of our computed sticking probabilities to the molecular beam experiments and the causes for discrepancies between theory and experiment. Conclusions are provided in Section 2.4.

TABLE 2.1: The exchange-correlation functionals used in this work.

Name	Type	Exchange	Correlation
PBEα = 0.57-vdW-DF2	vdW-DF	PBEα[38]	vdW-DF2[37]
PBEα = 1.25-vdW-DF2	vdW-DF	PBEα[38]	vdW-DF2[37]
PBE-vdW-DF2	vdW-DF	PBE[10]	vdW-DF2[37]
SRPB86R-vdW-DF2	vdW-DF	0.68B86R[39]+0.32RPBE[40]	vdW-DF2[37]
SRP0.5-vdW-DF2	vdW-DF	0.5RPBE[40]+0.5PBE[10]	vdW-DF2[37]
SRP0.32-vdW-DF2	vdW-DF	0.32RPBE[40]+0.68PBE[10]	vdW-DF2[37]
SRP0.5-vdW-DF1	vdW-DF	0.5RPBE[40]+0.5PBE[10]	vdW-DF1[36]
SRP48	GGA	0.48RPBE[40]+0.52PBE[10]	PBE[10]
PBE	GGA	PBE[10]	PBE[10]

2.2 Methods

2.2.1 Dynamical model

In all calculations, we used the Born-Oppenheimer static surface (BOSS) model[4]. For reasons that we mentioned earlier in our introduction, this approximation is good enough to describe the reaction of H_2 on a metal surface. We neglect the degrees of freedom of the surface atoms and only the H_2 degrees of freedom (6D) are taken into account. Fig. 2.2a depicts the coordinate system used for the dynamics and Fig. 2.2b the surface unit cell for the Ni(111) system and the high symmetry impact sites.

2.2.2 Construction of the PES

For the full (6D) PES construction, self-consistent DFT was used, applying the candidate SRP functionals listed in table 2.1 to try and obtain chemical accuracy. The main idea of SRP-DFT as first proposed by Díaz et al.[4] is that the exchange-correlation (XC) functional is adapted to the system at hand by optimizing the α parameter in Eq. (2.1)

$$E_{\mathrm{XC}} = \alpha E^1_{\mathrm{XC}} + (1-\alpha)E^2_{\mathrm{XC}}. \tag{2.1}$$

Here, E^1_{XC} and E^2_{XC} are two "standard" (i.e GGA level) XC functionals, of which one generally tends to overestimate the sticking coefficient, and the second tends to underestimate the sticking coefficient. Standard XC functionals used for molecule-surface reactions are the PBE[10] and RPBE[40] functionals. Downsides of the SRP-approach are that the approach is specific to one system, one needs at least one experimental data set to construct an SRP-DF, and the quality of this functional depends on the quality of the experiment.

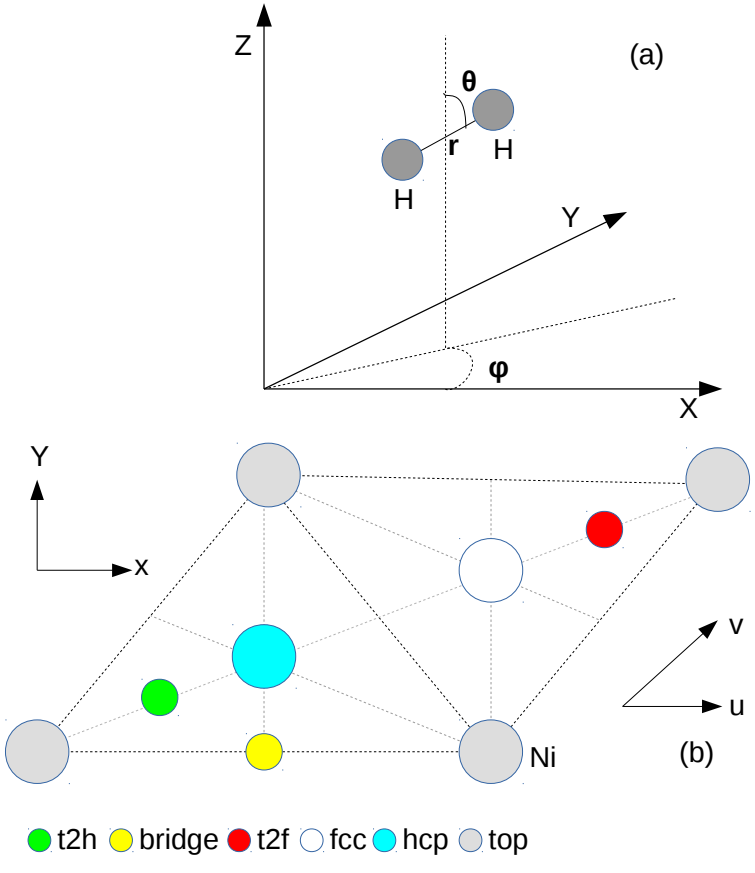

FIGURE 2.2: (a) Coordinate system used to describe the H_2 molecule relative to the static Ni(111) surface. (b) The surface unit cell and sites considered for the Ni(111) surface. The origin `(X=u=0,Y=v=0,Z=0)` of the center of mass coordinates is located in the surface plane at a top site, i.e., at a surface atom.

As found to be necessary for CHD_3 on Ni(111)[41], CHD_3 + Pt(111)[42,43], H_2 + Pt(111)[35], and H_2 on Ru(0001)[44], in many cases we take the correlation functional to describe the van der Waals interaction using the correlation functional of Dion et al.[36](E_C^{vdW-DF}) or Lee et al.[37]($E_C^{vdW-DF2}$). These correlation functionals have been shown to improve the description of weakly activated dissociation[44] while maintaining the same accuracy[45] or improving the accuracy[41] for highly activated dissociation systems. The PBEα=0.57-vdW-DF2 functional is the SRP-DF for the chemically related H_2 + Pt(111) system[35], which suggests that it might also work well for H_2 + Ni(111).

The vdW-DF1 and vdW-DF2 correlational functionals are non-empirical, being based on first principles. With their inclusion, our SRP functional form becomes

$$E_{\mathrm{XC}} = \alpha E_{\mathrm{X}}^{1} + (1-\alpha) E_{\mathrm{X}}^{2} + E_{\mathrm{C}}. \tag{2.2}$$

In equation (2.2), the contributing exchange functionals E_X and the correlation functionals E_C included in the exchange-correlation functionals we used are specified in Table 2.1.

To solve the Kohn-Sham equations, we used the Quantum Espresso package (QE)[46]. In the calculations to construct PESs, we used the spin-polarized extension of the vdW-DF and vdW-DF2 correlation functional[47] implemented in QE. Furthermore, we implemented the exchange part of the SRPα-vdW-DF(or vdW-DF2) functional through the modified version of the LIBXC exchange-correlation functional library[48]. The electron-ion interaction is described by using the projector augmented wave (PAW) potentials as proposed by Blöchl[49] from the pseudopotential library[50](version 1.0.0) with the energy cut off for plane wave expansion corresponding to 50 Ry (1 Ry≈13.606 eV) with 0.011025 Ry wide Methfessel-Paxton smearing to facilitate the convergence. The Brillouin zone has been sampled with a 5×5×1 Γ-centered grid of k-points. We used a (3×3) surface unit cell with a total of 36 Ni atoms, with 18 Å vacuum separating the slab from its first periodic image, and a 4 layers slab.

We first optimized the geometric structure of the Ni slab with the Vienna *ab initio* simulation package (VASP) package[51,52]. First, the bulk fcc lattice constant was determined using a 24×24×24 Γ-centered grid of k-points. Next, slab relaxation calculations were performed using a 24×24×1 Γ-centered grid of k-points and the energy cut off for plane wave expansion corresponding to 400 eV and 0.1 eV wide Methfessel-Paxton (or Fermi) smearing for convergence. After having obtained the relaxed slab (see Table S1 of the Supporting Information (SI) of Ref.[53] for the results of the PBE-vdW-DF2 functional), the convergence of the molecule-surface interaction energy has been tested with respect to the

number of metal layers, cell size, the cut-off energy and the k-point sampling by comparing computed minimum energy barrier heights. The transition state (TS) geometries have been determined using the dimer method as implemented in the VASP transition state tools (VTST) package[54–57]. In the TS search, the surface was frozen in the relaxed 0 K geometry of the bare slab. The optimization of the TS geometries has been stopped once the maximum force on any degree of freedom was smaller than 5 meV/Å. All the TS geometries have been proven to be first order saddle points in the molecular coordinate space through frequency analysis (by checking that one and only one imaginary frequency was found). The barrier height has been computed as $E_b = E_{TS}$-E_{asym}; here E_{TS} is the absolute energy of the transition state geometry and E_{asym} is the absolute energy of the system with the molecule in the gas phase. The gas phase geometry consists of the optimized molecule placed in the vacuum far from the surface. For our case, the vacuum distance was 18 Å and the gas phase molecule was taken at 9 Å from the slab. Note that the TS geometries presented in Section III were obtained from the PESs fitted to data computed with QE. We ascertained that the molecule-surface interaction energies calculated with VASP (in convergence tests) were in good agreement with those computed with QE (used for PES fitting and dynamics), see Table S2 of the SI of Ref.[53].

2.2.3 Interpolation of PES

The PESs were interpolated using the corrugation reducing procedure (CRP)[58,59], with the formula

$$V^{6D}(\overrightarrow{r}) = I^{6D}(\overrightarrow{r}) + \sum_{i=1}^{2} V_i^{3D}(\overrightarrow{r_i}) \tag{2.3}$$

in which V^{6D} is the full 6D PES of the H_2/surface system, $\overrightarrow{r}$ is the vector of coordinates of the H_2 molecule with respect to the surface, I^{6D} is the so-called 6D interpolation function of the H_2/surface system, V_i^{3D} is the 3D PES of the H/surface system and $\overrightarrow{r_i}$ is the vector of coordinates of the *ith* H atom with respect to the surface. The 3D atom-surface PES is then written as

$$V_i^{3D}(\overrightarrow{r_i}) = I_i^{3D}(\overrightarrow{r_i}) + \sum_{j=1}^{N} V^{1D}(\overrightarrow{R_{ij}}) \tag{2.4}$$

where I_i^{3D} is the 3D interpolation function describing the H/surface system, N is the number of surface atoms taken into account, V^{1D} is the 1D functional mimicking the interaction of the H atom with a single surface atom and R_{ij} is the distance between H atom i and surface atom j.

The idea behind the CRP is to interpolate the I^{6D} instead of V^{6D}, as I^{6D} is much less corrugated in the u, v, θ and φ degrees of freedom than V^{6D} is[58]. The (u,v) coordinate system is a coordinate system in which the surface lattice vectors are taken as unit vectors(Fig. 2.2).

For H_2 on Ni(111), the skewing angle of the coordinate system is 60^0 (Fig. 2.2b). The interpolation procedure used for the C_{3v} potential of H_2+Ni(111) is the same as used in Ref.[44] for H_2 on Ru(0001) and for H_2+Cu(111) and H_2+Pt(111)[45]. For the interpolation of the I^{6D} potential with C_{3v} symmetry, 29 configurations of (u, v, θ, φ) are used, spread over six differents sites (u, v). These sites are shown in Fig. 2.2b. The configurations used in this work are exactly the same as used in Ref.[44], see also Tables S3 and S4 of the SI of Ref.[44].

The interpolation is done in several steps: First, for every configuration, the interpolation is performed over the r and Z degree of freedom. For this interpolation, a 15×26 ($r \times Z$) grid is used, employing a two-dimensional (2D) cubic spline interpolation, where r_{min} = 0.4 Å, r_{max} = 2.3 Å, Z_{min} = 0.25 Å and Z_{max} = 6.5 Å. Then, for every site, the interpolation is performed over the θ and φ degrees of freedom using symmetry-adapted products sin and cos functions. Finally, an interpolation over u and v is performed, for which again symmetry-adapted products sin and cos functions are used. At long-range, we apply a switching function between 5.5 Å and 6.5 Å from the full 6D potential to a 2D asymtotic gas-surface potential that only depends on r and Z, because far away from the surface, the corrugation and anisotropy of the PES are vanishingly small. This asymtotic potential is represented by

$$V^{2D}(r, Z) = V^{ext}(Z) + V^{gas}(r) \tag{2.5}$$

where V^{ext} is a function describing the dependence of the PES on Z beyond Z = 6.5 Å and V^{gas} is the interaction at $Z = Z_{max}$ = 9 Å. For the I^{3D} interpolation, 10 sites in (u, v) are used for the potentials with C_{3v} symmetry. The 10 sites used in this work are exactly the same as used in Ref.[44]. Apart from the top site where 202 points are taken in Z, for each site 106 points are taken in Z, with Z_{min} = -1.195 Å and Z_{max} = 9 Å. The function V^{1D} is taken to describe the interaction of the H atom with the surface above the top site, as used previously for the investigation of H_2+Cu(111)[45].

2.2.4 Dynamics Methods

2.2.4.A Quasi-classical Dynamics

We take into account the zero-point energy of H_2 to compute the dynamical observables by using the QCT method[60]. To evaluate the initial state-resolved

reaction probabilities, we placed our molecule initially at $Z = 9$ Å with a velocity normal toward the surface that corresponds to a specific initial incidence energy. At this distance, the interaction of the molecule with the surface is essentially zero. For each average beam translational energy, accurate results were obtained with typically 40,000 trajectories. In all cases, the maximum propagation time is 2 ps. To propagate our equation of motions, the Stoer and Bulirsh[61] method was used. The time-independent Schrödinger equation was solved using the Fourier grid Hamiltonian method[62] to determine the bound state rotational-vibrational eigenvalues of gas phase H_2. The bond distance and the vibrational velocity of the molecule are randomly sampled from a one-dimensional quasi-classical dynamics calculation of a vibrating H_2 molecule for the corresponding rovibrational energy[63]. The orientation of the molecule, θ and φ, is chosen also based on the selection of the initial rotational state. The magnitude of the classical initial angular momentum is fixed by $L = \sqrt{j(j+1)}/\hbar$ and its orientation, while constrained by $\cos\Theta_L = m_j/\sqrt{j(j+1)}$, is otherwise randomly chosen as described by Wijzenbroek et al.[45] . Here, j is the rotational quantum number, m_j the magnetic rotational quantum number and Θ_L the angle between the angular momentum vector and the surface normal. Other initial conditions are randomly chosen as described in Ref.[63].

2.2.4.B Quantum Dynamics

The time-dependent wave packet (TDWP) method was used[64] for the quantum dynamical (QD) calculations. The Fourier representation[65] was used to represent the wave packet in Z, r, X, and Y. We employed a finite basis representation to represent the angular wave function[66,67]. The time-dependent Schrödinger equation was propagated using the split operator method[68]. The initial wave packet is taken as a product of a Gaussian wave packet describing the motion of the molecule towards the surface, a plane wave function for motion parallel to the surface, and a rovibrational wave function to describe the initial vibrational and rotational state of the molecule. The scattering amplitude formalism[69–71] is used to analyse the reflected wave packet at $Z = Z_\infty$. Z_∞ is a value of Z (9 Å) where there is no interaction between the molecule and the surface. An optical potential is used to absorb the reacted(r) or scattered(Z) wave packet for large values of r and Z[72]. For full details of the method and equations, see Ref.[73]. The parameters used in this work are given in Table S5 of the SI of Ref.[53].

2.2.5 Computation of the Observables

2.2.5.A Degeneracy-Averaged reaction probabilities

In our QCT calculation of the reaction probabilities, we considered our molecule dissociated when its H-H distance becomes greater than 2.0 Å. Otherwise, the H_2 molecule is considered to be reflected from the surface to the gas phase when its distance to the surface in Z exceeds 6.5 Å and H_2 has a velocity toward the vacuum. The reaction probability was calculated as the ratio of the number of dissociated trajectories, using the formula

$$P_{\mathrm{r}} = N_{\mathrm{r}}/N_{\mathrm{total}} \tag{2.6}$$

where N_{total} is the total number of trajectories and N_{r} is the number of reactive trajectories. The degeneracy-averaged reaction probability for a particular initial vibrational state ν and rotational state j can be computed as

$$P_{\mathrm{deg}}(E_i;\nu,j) = \sum_{m_j=0}^{j} (2-\delta_{m_j}) P_{\mathrm{r}}(E_i;\nu,j,m_j)/(2j+1). \tag{2.7}$$

Here, P_{r} is the fully initial-state-resolved reaction probability. P_{r} can be computed with the TDWP method from

$$P_{\mathrm{r}}(E_i;\nu,j,m_j) = 1 - \sum_{\nu',j',m'_j,n,m} P_{\mathrm{scat}}(E_i;\nu,j,m_j \to \nu',j',m'_j,n,m) \tag{2.8}$$

P_{scat} are the state-to-state scattering probabilities from the initial state (ν,j,m_j) to the final state (ν',j',m'_j,n,m), where n and m are the quantum numbers for diffraction.

2.2.5.B Molecular Beam sticking probabilities

When calculating the sticking probabilities using a molecular beam simulation, the properties of the experimental molecular beam should be taken into account. This is done in two steps : Firstly, the monoenergetic reaction probabilities $R_{\mathrm{mono}}(E_i,T_{\mathrm{n}})$ are computed through Bolzmann averaging over all rovibrational states populated in the molecular beam with the nozzle temperature T_{n} at the collision energy E_i[45] :

$$R_{\mathrm{mono}}(E_i,T_{\mathrm{n}}) = \sum_{\nu,j} F_{\mathrm{B}}(\nu,j,T_{\mathrm{n}}) P_{\mathrm{deg}}(E_i;\nu,j) \tag{2.9}$$

Here F_{B} is the Bolzmann weight of each (ν, j) state.

$$F_{\mathrm{B}}(\nu, j, T_{\mathrm{n}}) = \frac{w(j)F(\nu, j, T_{\mathrm{n}})}{\sum_{\nu', j' \equiv j(mod2)} F(\nu', j', T_{\mathrm{n}})} \tag{2.10}$$

in which

$$F(\nu, j, T_{\mathrm{n}}) = (2j+1)\exp(-E_{vib}(\nu, j))/k_B T_{vib}) \\ \times \exp(-E_{rot}(\nu, j))/k_B T_{rot}) \tag{2.11}$$

In equation (2.10), the summation runs only over the values of j' with the same parity as j. In equation (2.11) E_{vib} and E_{rot} are the vibrational and rotational energy, respectively, of the (ν, j) state and k_B is the Bolzmann constant. In these equations, it is assumed that the rotational temperature of the molecules in the beam is lower than the nozzle temperature ($T_{\mathrm{rot}} = 0.8\ T_{\mathrm{n}}$)[74,75] and that the vibrational temperature is equal to the nozzle temperature ($T_{\mathrm{vib}} = T_{\mathrm{n}}$). We also assume that the fractions of ortho- and para-H_2 and D_2 are equivalent to those in the high-temperature limit, given by $w(j)$. For H_2, $w(j)$ is equal to $\frac{1}{4}$ for even j and $\frac{3}{4}$ for odd j, and for D_2, $w(j)$ is equal to $\frac{2}{3}$ for even j and $\frac{1}{3}$ for odd j.

Secondly, the experimental spread of incidence energies is taken into account. The monoenergetic reaction probability is averaged over the velocity distribution by[76]

$$R_{\mathrm{beam}} = \frac{\int_0^\infty f(v_i; T_{\mathrm{n}}) R_{\mathrm{mono}}(E_i; T_{\mathrm{n}}) dv_i}{\int_0^\infty f(v_i; T_{\mathrm{n}}) dv_i} \tag{2.12}$$

Here, $f(v_i; T_{\mathrm{n}})$ is the flux-weighted velocity distribution, which is given by[77]

$$f(v_i; T_{\mathrm{n}}) = C v_i^3 \exp[-(v_i - v_0)^2/\alpha^2] \tag{2.13}$$

In equation (2.13), C is a constant, v_i is the velocity of the molecule, v_0 is the stream velocity, and α is a parameter describing the width of the velocity distribution. The v_0 and α used in our calculations (Table 2.2) where obtained by fitting the experimental time of flight (TOF) spectra[78] characterising H_2 beams used in the Rendulic group to the function

$$G(t; T_{\mathrm{n}}) = c_1 + c_2 v_i^4 \exp[-(v_i - v_0)^2/\alpha^2] \tag{2.14}$$

using the Levenberg-Marquardt algorithme[79].

TABLE 2.2: Parameters used for the molecular beam simulations of H_2 on Ni(111). The parameters were obtained from fits of equation (2.14) to the experimental time of flight spectra[78]. Also presented is the Bolzmann population of the ($\nu = 0, j = 0$) state of H_2 in the beam.

$T_n(K)$	$<E_i>(eV)$	c_1	$c_2 \times 10^{-15}$	$v_0(m/s)$	$\alpha(m/s)$	F_B ($\nu = 0, j = 0, T_n$)
100	0.035	0.021	0.753	1,832.40	82.31	0.24788
300	0.067	0.009	0.238	2,496.08	239.45	0.15560
500	0.122	0.023	8.069	3,127.77	740.22	0.09853
800	0.153	0.023	5.570	3,352.75	1,005.88	0.06291
1100	0.216	0.041	3.120	3,679.94	1,464.91	0.04589
1400	0.303	0.018	2.172	3,650.40	2,237.06	0.03575
1700	0.392	0.016	57.918	3,320.96	2,998.75	0.02891

2.3 Results and Discussion

2.3.1 Potential Energy Surfaces

Fig. 2.3 shows, for some selected high symmetry configurations, two-dimensional (2D) cuts through the PESs (also called elbow plots) for the PBE-vdW2 and for the PBE functionals. In all cases, H_2 was oriented parallel to surface. In agreement with the previous work on H_2 on Ru(0001)[44], the barrier height decreases in the order hcp/fcc>bridge>t2h/t2f>top (see Table 2.3). The hcp barrier was found to be slightly lower than the fcc barrier. With the PBE-vdW2 functional, the dissociation is activated, in the sense that the transition states have as energies 24 meV and 135 meV for the early barrier and late barrier, respectively, above the top site (Fig. 2.3(a)). With PBE, the dissociation is very weakly activated with the energies of 11 meV for the early and -180 meV for the late barrier (Table 2.3). Non-activated behaviour was observed for the PBEα0.57-vdW2 functional (see Table S6 of the SI of Ref.[53]) with energies of -50 meV and -27 meV for the early and late top site barriers, respectively. For the other functionals, the dissociation was found to be activated (see Table S6 of the SI of Ref.[53]).

From Fig. 2.3, we can also see that, for the PBE-vdW2 functional, the top and t2f symmetry configurations present two saddle points, with a local minimum in between (Figs. 2.3a and 2.3d). This notable feature is general for all functionals except for the PBE, the SRP48 functional and for SRPB86R-vdW2 where the PES was found to exhibit only one saddle point for the t2f configuration (see Table S6 of the SI of Ref.[53] and Fig. 2.3h). Differences were found with respect to the relative energies of the early and late barriers present in 2D cuts above the top and t2f impact sites. Note that, when using the PBEα functional[38] with α being the adjustable parameter, if $\alpha = 1$, the PBEα functional corresponds to the PBE[10] functional, while for $\alpha \to \infty$, the PBEα functional corresponds to the RPBE[80] functional. For PBEα-vdW2 and SRPα-vdW1 (vdW2), the late barrier

TABLE 2.3: Some selected barrier heights (in eV) and locations (r_b,Z_b) (in Å), relative to the gas phase minimum, for the four geometries depicted in Fig. 2.3 and for hcp. Where available, energy barriers have been indicated for the PBE-vdW2 and PBE funtionals. All geometries are for the H_2 molecule lying parallel to the surface ($\theta = 90^0$).

Parameters	top(early)	top(late)	brg	hcp	fcc	t2f(early)	t2f(late)
φ	0^0	0^0	90^0	30^0	0^0	240^0	240^0
$Z_b^{PBE-vdW2}$	2.083	1.368	1.602	1.519	1.508	1.747	1.304
Z_b^{PBE}	2.349	1.372	1.838	1.741	1.731	2.034	-
$r_b^{PBE-vdW2}$	0.763	1.240	0.810	0.843	0.847	0.790	1.021
r_b^{PBE}	0.763	1.222	0.794	0.811	0.812	0.777	-
$E_b^{PBE-vdW2}$	0.024	0.135	0.321	0.412	0.427	0.174	0.162
E_b^{PBE}	0.011	-0.180	0.179	0.248	0.257	0.089	-

for the top symmetry configuration was found to be higher than the early top site barrier, in contrast with the SRP48, PBE and SRPB86R-vdW2 functionals where the opposite was found (See Table S6 of the SI of Ref.[53]). The latter 3 functionals also correspond to the functionals for which only an early barrier is found on the t2f site.

To gain a deeper understanding of the PESs' features, we also consider here the energetic corrugation, as was done previously[44] in an investigation of H_2 on Ru(0001). The energetic corrugation is defined as the difference between the hcp($\theta = 90^0$, $\varphi = 30^0$) barrier height and the earlier top site ($\theta = 90^0$, $\varphi = 0^0$) barrier height. The energetic corrugation corresponds to the width of the reaction probability curve for an activated dissociation system[44,81]. It usually corresponds to the range of energies over which the reaction probability increases more or less linearly from an onset energy that is close to the reaction threshold to an energy at which the reaction probability starts to plateau[44]. Fig. 2.4A plots the energetic corrugation against the top site barrier height and Fig. 2.4B depicts the variation of the early barrier height above the top site against the distance to the surface of this early barrier. For the most part, we observe a linear dependence for functionals with the same correlation functional, as seen for PBEα-vdW2, where the corrugation energetic increases with the α parameter. Specifically, the functionals with higher top barrier heights tend to yield a larger energetic corrugation if they have the same correlation functional. This is the case for the SRPα-vdW2 functionals. The early top site barriers tend to be closer to the surface if van der Waals correlation is used (Fig. 2.4B), and, more generally, the barriers get closer to the surface if PBE correlation is replaced by vdW2 (see Table 2.3) or vdW1 correlation. This is why functionals yielding similar early

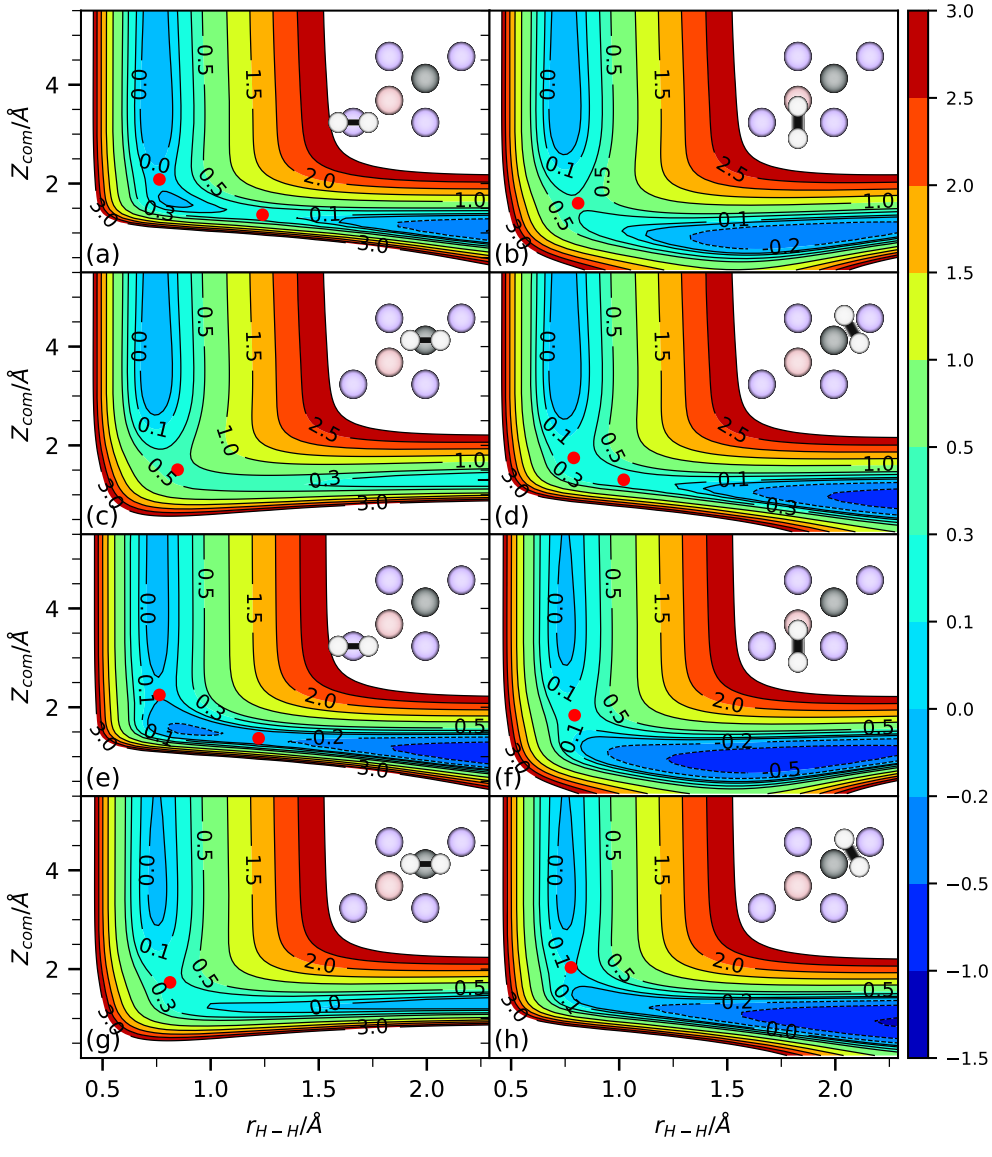

FIGURE 2.3: Elbow plots (i.e: V(Z,r)) of H_2 on Ni(111) for four high symmetry configurations with H_2 parallel to the surface (θ=90^0) computed with PBE-vdW2[(a), (b), (c) and (d)] and PBE[(e), (f), (g) and (h)] functionals and interpolated with CRP method, for the top(φ=0^0), bridge(φ=90^0), fcc(φ=0^0) and t2f(φ=120^0) configurations shown in the insets. Saddle points are indicated by red circles.

top site minimum barriers tend to yield a larger energetic corrugation if they incorporate van der Waals correlation instead of PBE correlation, as also seen in Fig. 2.4A and previously found for H_2 + Ru(0001). Increasing the α-parameter makes the functionals more repulsive, leading to early barriers that are further from the surface. The trends observed in Fig. 2.4 were previously found for H_2 on Ru(0001)[44].

2.3.2 Comparison to experiment

In Fig. 2.5, the sticking probabilities (S_0) computed with molecular beam simulations for H_2 dissociating on Ni(111) are shown for all functionals used, and compared with the experiments of Rendulic et al.[28]. From panel (a), we see that the S_0 computed with PBE[10] are in reasonable agreement with the sticking coefficients computed in fully classical simulations with PW91[33,34] by Kresse. Differences may be attributed to the different simulation methods used, small differences in the functionals (but note that the PBE functional was designed to reproduce PW91 energies closely[10]), and differences in the input parameters to the DFT calculations. For instance, Kresse performed fully classical simulations, choosing the rovibrational energies according to incidence energy, while we performed QCT simulations with averaging over the beam's translational energy distribution and rovibrational state populations.

The PBE[11] functional overestimates the sticking probability. This clearly indicates that the highest top site barrier found for the PBE PES (11 meV) is too low. On the other hand, the SRP50-vdW2(RPBE:PBE(50:50)vdW2) functional consistently underestimates the measured S_0. This clearly suggests that the barriers in this PES are too high. Results for the SRP32-vdW2 functional closely resemble those of the SRP50-vdW2 functional and are therefore not shown in Fig. 2.5. If we replace the vdW2 correlation from SRP50-vdW2 by PBE correlation and slightly change the α parameter (SRP48), both the reaction threshold and the width of the sticking probability curve change. The reaction probability is underestimated for $E_i < 0.2$ eV and overestimated for $E_i > 0.2$ eV. If on the other hand we only change the exchange part to a mixture of B86R[39] and RPBE[80] exchange while keeping vdW2 correlation (B86R:RPBE(68:32)vdW2), we obtain a sticking probability curve that is very similar to the one obtained with SRP48. Neither the SRP48 nor the B86r:RPBE(68:32)-vdW2 functional yield good agreement with experiment. Both functionals containing PBE correlation (PBE and SRP48) yield sticking curves that are too steep at the onset to yield good agreement with experiment at the onset of the experimental sticking curves.

As Fig. 2.5(b) shows, the PBEα = 0.57-vdW2 functional also leads to a consistently overestimated sticking probability. The extrapolation of the

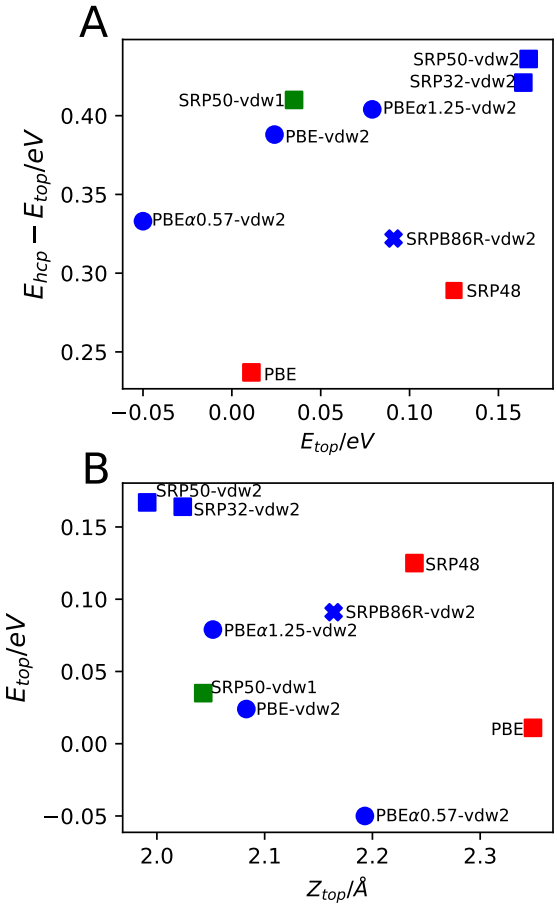

FIGURE 2.4: (A) Energetic corrugation of the potential versus the barrier height associated with the early top site barrier for the constructed PESs for the functionals investigated. (B) Height of the early top to bridge barrier versus the distance of the surface of the early top to bridge barrier for the constructed PESs for the functionals investigated. Results obtained with functionals sharing the same correlation functional are shown with the same colour. Results obtained with functionals using a similar expression for the exchange functional in Eq. 2.2 are shown with the same symbol (i.e., blue vdW2, green vdW1, red PBE for correlation; square mix PBE:RPBE, circle PBEα, cross mix B86R:RPBE for exchange).

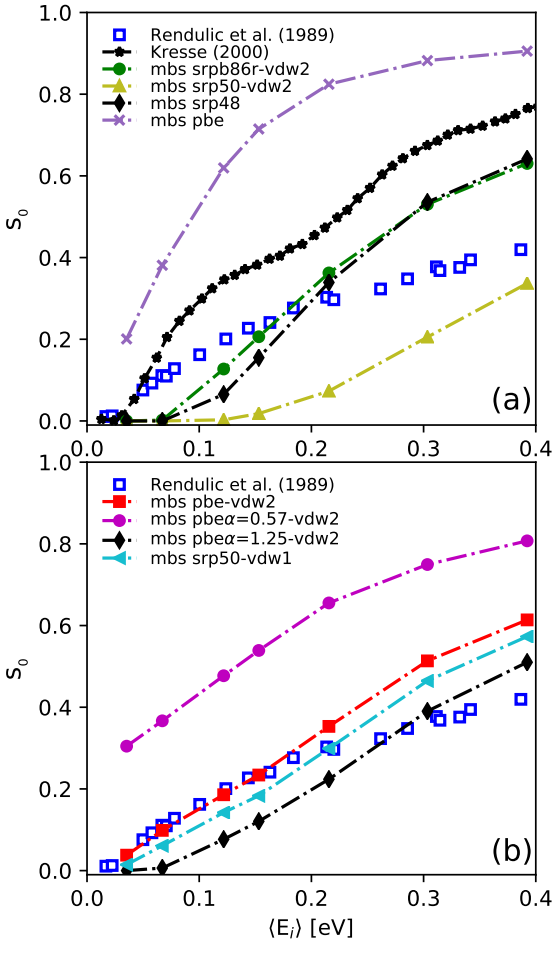

FIGURE 2.5: (a,b) Reaction probability for moleculars beams of H_2 dissociating on Ni(111) computed with various functionals, compared to experiment[28].

computed reaction probability curve to lower incidence energies yields a positive intercept, in agreement with our finding that with this functional reaction is non-activated above the top site, but in disagreement with experiment. The results show that the PBE$\alpha = 0.57$-vdW2 functional is not transferable from H_2 + Pt(111)[35] to H_2 + Ni(111).

With the PBE-vdW2(PBE$\alpha = 1.0$-vdW2) PES, excellent agreement with experiment is achieved at the lowest incidence energies (up to 0.2 eV), but the computed S_0 are too high in the higher energy range (0.2-0.4 eV). Nevertheless it is encouraging that the agreement is good for the incidence energy range for which good agreement was found in the experiments of Rendulic et al.[28], Resch et al.[29], and of Hayward and Taylor[27]. In particular, we note that replacing PBE correlation with vdW2 correlation in the PBE functional (thus obtaining PBE-vdW2) leads to a sticking curve that has not only the correct onset, but also the correct shape (steepness) for incidence energies up to about 0.2 eV. A similar finding was previously obtained for H_2 + Ru(0001)[44]. From Fig. 2.5(b), we can also see how the computed S_0 curve depends on the α parameter when using PBEα exchange and vdW2 correlation. The S_0 curve shifts to higher E_i when the α parameter increases, but the shape of the S_0 curve is basically unchanged. With the PBE$\alpha = 1.25$-vdW2 functional, the computed S_0 are too low for E_i up to 0.25 eV and too high for $E_i > 0.3$ eV. Finally, the RPBE:PBE(50:50)vdW1 (SRP50-vdW1) functional also gives reasonable agreement with experiment, with the computed S_0 being rather similar to those obtained with the PBE-vdW2 functional. These two functionals were also found to give good agreement with one another and with experiment for the weakly activated dissociation of H_2 on Ru(0001)[45].As also found for this system, the PBE-vdW2 and SRP50-vdW1 functionals yield a similar minimum barrier height and energetic corrugation (Fig. 2.4A). If we put emphasis on the comparison to the experimental data of Rendulic et al.[28] for energies up to 0.2 eV, the PBE-vdW2 functional is best, followed closely by the SRP50-vdW1 functional.

Having arrived at our verdict on which functional is most accurate when comparing to the results of Rendulic et al.[28], we now perform a more extensive comparison with available experiments to arrive at a verdict on the quality of the PBE-vdW2 functional for describing H_2 + Ni(111). In Fig. 2.6 we compare our computed S_0 for this functional to experimental S_0 for normal and off-normal incidence obtained by Rendulic et al.[28] and to experimental S_0 for normal incidence obtained by Resch et al.[29] . As was the case for the normal incidence results obtained by Rendulic et al. (Fig. 2.6b), their results for off-normal incidence (Fig. 2.6c) start to deviate from the computed S_0 for $E_i > 0.2$ eV. As the S_0 measured by Rendulic et al. obeyed normal energy scaling, this can be taken to suggest that the discrepancies between the PBE-vdW2 theory and

experiment at $E_i > 0.2$ eV could be due to differences between the translational energy distributions used in the experiments and in the simulations, a point we will come back to below.

For normal incidence the S_0 computed with PBE-vdW2 are in better agreement with the results of Resch et al. (Fig. 2.6a) than with those of Rendulic et al. (Fig. 2.6b). Both experimental data sets were obtained in the same group (of Rendulic). Assuming the results obtained later to be the most accurate, we will therefore base our verdict on the quality of the PBE-vdW2 functional on the comparison in Fig. 2.6a. We do this in the usual way[13,14,82] by computing the mean absolute deviation (MAD) between theory and experiment, which is computed as the average of the absolute difference in incidence energy between the experimental S_0 and the theoretical sticking probability curve spline interpolated to that value of S_0 (some examples of incidence energy differences are shown in Fig. 2.6). The MAD values and also values of the mean signed difference (MSD) are reported in Table 2.4. As can be seen, the MAD value for the comparison with the normal incidence data of Resch et al. is 26 meV (0.60 kcal/mol), i.e., lower than 1 kcal/mol. Therefore, from this point of view the PBE-vdW2 functional is a candidate SRP density functional for H_2 + Ni(111). This statement comes with the following three caveats: (i) Our only criterion for taking the experimental dataset from normal incidence by Resch et al. as the reference data set has been that these data were obtained later in time and in the same group as the data of Rendulic et al., (ii) when the comparison is made with the normal incidence data of Rendulic et al., we do arrive at an MAD value (1.42 kcal/mol) greater than 1 kcal/mol, and (iii) for a candidate SRP-DF to be called a true SRP-DF it should also describe an experiment on H_2 + Ni(111) to which it was not fitted with chemical accuracy. Here, the experiment of Rendulic et al. for $\theta = 40^0$ does not count, one reason being that it is not independent from the normal incident experiment the PBE-vdW2 functional was fitted to (because normal and off-normal incidence results are related by normal energy scaling[28]).

For the PBE-vdW2 functional to be called an SRP-DF, we think two things should happen: (i) new and well-defined experiments should be carried out on sticking of H_2 to Ni(111) for $E_i > 0.2$ eV to clear up the energy dependence of sticking at larger incidence energies, and (ii) the quality of the PBE-vdW2 functional should be confirmed through a successful comparison with another experiment probing the H_2-Ni(111) interaction. Our present results do suggest that the PBE-vdW2 functional describes the minimum barrier region of the PES accurately. In the next section we will discuss possible explanations of the discrepancies that remain between the PBE-vdW2 theory and the experiments for $E_i > 0.2$ eV.

TABLE 2.4: MAD and MSD values characterizing the agreement between the S_0 computed with the PBE-vdW2 functional and measured in experiments.

Experiment	MAD (kcal/mol)	MSD (kcal/mol)
Resch et al.[29], $\theta = 0^0$	0.60	0.60
Rendulic et al.[28], $\theta = 0^0$	1.42	1.34
Rendulic et al.[28], $\theta = 40^0$	0.90	0.37

2.3.3 Causes for the discrepancies between theory and experiment

To understand the discrepancy between the experiments and the best theoretical (PBE-vdW2) results at the highest energies mentioned above, we discuss four potential sources of error:(i) errors in the experiments; (ii) errors in the simulation of the experiments due to assuming wrong translational energy distributions or nozzle temperatures; (iii) errors in the dynamical model or dynamics method used, and (iv) errors in the PES used.

As we mentioned earlier in our introduction, many sets of experimental data have been published on sticking of H_2+Ni(111). The sets of measurements from Rendulic et al.[28], Resch et al.[29] and Hayward and Taylor[27] are in reasonable agreement with one another for low incidence energies, and the discrepancies between the first two experiments for incidence energies > 0.2 eV may point to problems with the experiments at these energies (Fig. 2.1). As can be seen from the normal incidence results in Figs. 2.6a and 2.6b, at the higher energies better agreement is obtained of the PBE-vdW2 results with the set of S_0 published later by the Rendulic group (in 1993, by Resch et al.). Again assuming the results obtained later in time to be more accurate, this might be taken to suggest that the S_0 measured by Rendulic et al. were too low for $E_i > 0.2$ eV. This might be related to the translational energy distributions of the beam, as suggested by the observation that our computed S_0 for PBE-vdW2 are also too high for off-normal incidence with $E_i > 0.2$ eV when comparing to the data of Rendulic et al. (Fig. 2.6c).

In Fig. 2.7, we have also plotted the S_0 measured by Resch et al.[29] for adsorption of H_2 on Ni(111) covered by 0.02ML potassium. It is clear that at incidence energies > 0.25 eV, the experimental S_0 from Resch et al.[29] for the potassium covered surface reproduce those from Rendulic et al.[28] for the clean surface. As already pointed out, the experimental data from Resch et al.[29] for the clean Ni(111) surface reproduce our PBE-vdW2 results rather well, except for one point at 0.33 eV. While it may be tempting to attribute the

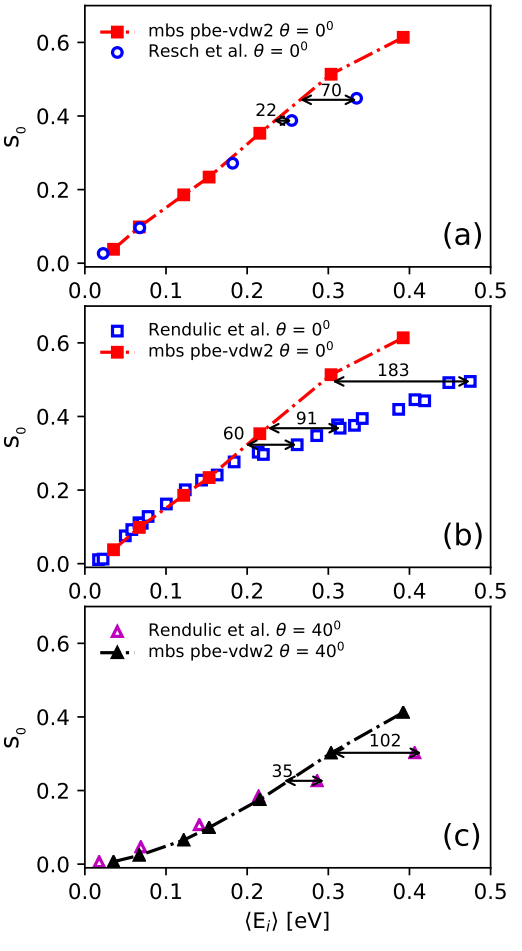

FIGURE 2.6: Sticking probability for moleculars beams of H_2 dissociating on Ni(111) computed with PBE-vdW2, compared to experiments[28,29] for H_2 normal and off-normal to Ni(111) surface. The numbers added to the arrows indicates differences in incidence energy between the experimental and interpolated theoretical S_0 in meV.

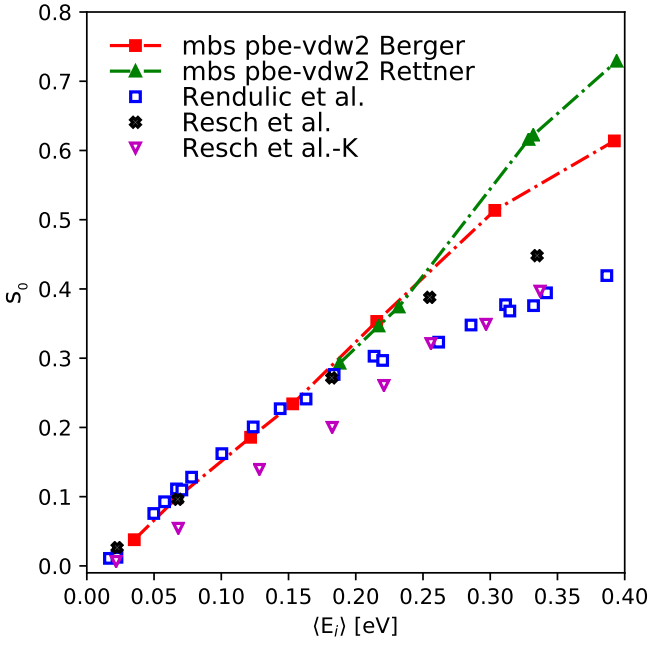

FIGURE 2.7: Comparison of reaction probability for moleculars beams of H_2 dissociating on Ni(111) computed with PBE-vdW2 and obtained with parameters from Berger[78](red square box) and from Rettner[74](green upper triangle), compared to experiments[28,29] for H_2 normal to Ni(111) surface.

discrepancies of the S_0 computed with PBE-vdW2 with the data of Rendulic et al. to contamination of their nickle sample with K in the experiments by Rendulic et al.[28], assuming a nickle surface covered by 0.02 ML K would lead to deteroriated agreement between the computed S_0 and the S_0 which would be measured for the covered surface for $E_i < 0.2$ eV. This suggests that contamination with K in the experiments is not the cause of the discrepancies we try to explain.

We now come to the second point, i.e, possible errors in the simulations of the molecular beam conditions. For neither set of measurements (Refs.[28,29]), the beam conditions have been published. Calculations on H_2+Cu(111)[4] have shown that the knowledge of the nozzle temperature and parameters characterising the translational energy distribution of the H_2 beam is essential for accurately simulating highly activated reactive scattering of H_2 from metal surfaces. In the absence of specified beam data, and as discussed above, in computing the S_0 discussed so far we have assumed that the beam parameters for H_2+Ni(111) were the same as those used in other experiments of this group, and obtainable from the Ph.D. thesis of Berger[78]. To investigate the sensitivity of the computed S_0 to the beam parameters, we also tested the beam parameters characterising pure H_2 beams from Rettner et al.[74] published in Refs.[4,83], which are characteristic of beams with a much narrower energy distribution[4]. As seen in Fig. 2.7, relative to the S_0 computed with the Berger beam parameters, the S_0 computed with the parameters due to Rettner and Auerbach and co-workers are higher for $E_i > 0.25$ eV. If anything, this suggests that the discrepancy with experiment is not due to simulating beams that are too narrow; rather, the experimental beams might have been broader in incidence energy than the Berger beams we simulated. An alternative explanation for the experimental S_0 being too low at large E_i is that the data collection time was too large in the King and Wells measurements to determine S_0, so that the measured S_0 no longer was equal to the initial sticking coefficient, but reflected sticking on an H-precovered surface.

We now turn to point (iii), the question of whether the dynamical method and the model used in our calculations might be responsible for the discrepancies with the experiment at higher incidence energies. We start by evaluating the quality of the QCT method for molecular beam simulations of the sticking probability. Quantum dynamical calculations have been carried out on H_2+Ni(111) reaction for normal incidence of H_2 in some selected initial rovibrational states. In Fig. 2.8, the degeneracy averaged initial state-resolved reaction probability obtained from QCT calculations is compared to QD results for $\nu = 0, j = 0$; $\nu = 0, j = 1$ and $\nu = 0, j = 2$, for the PBE-vdW2 functional. It is clear that, especially at the lowest energies, some oscillations are present in the QD results. These oscillations may be explained by the fact that the H_2 molecule has extra time to tunnel through the barrier when trapped in a metastable state leading to

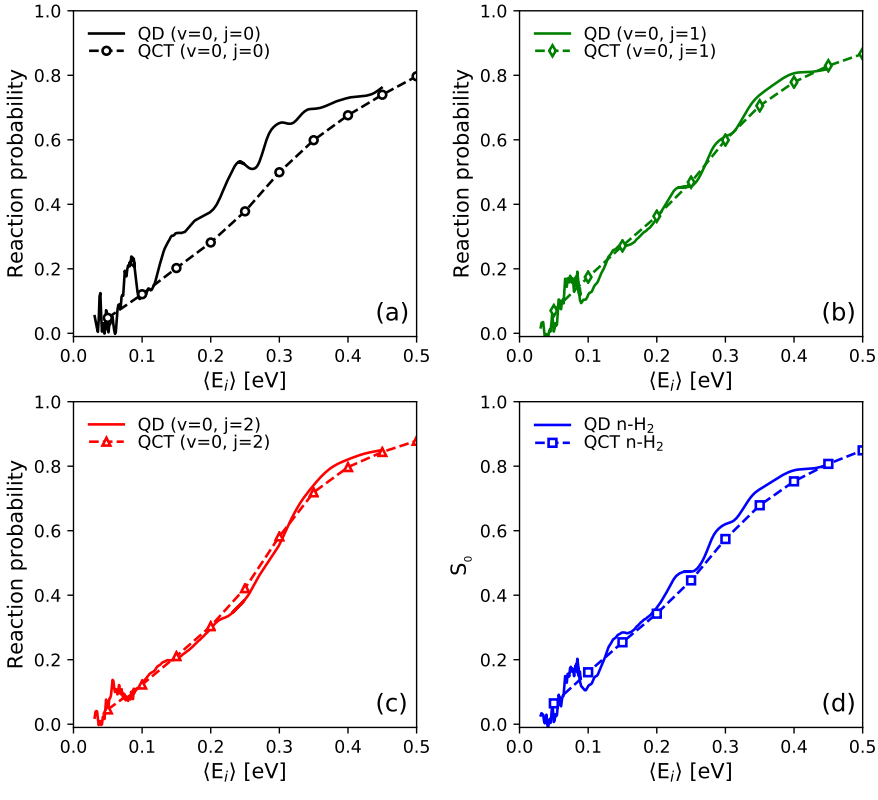

FIGURE 2.8: Comparison between quantum dynamics and quasi-classical trajectory for initial rotational state-resolved reaction probabilities of H_2 dissociating on Ni(111) computed with PBE-vdW2 (a-c), and comparison of sticking probability for cold n-H_2(d).

dissociation at the corresponding energies[84]. Our finding that the oscillations are most pronounced for the ($\nu = 0$,$j = 0$) state suggests that the trapping leading to the oscillations might be due to the population of excited librational (i.e., hindered rotational) states at the surface.

The agreement between QCT and QD is found to be excellent for the higher rotational states, i.e., for ($\nu = 0, j = 1$) and for ($\nu = 0, j = 2$). For ($\nu = 0, j = 0$), the QCT reaction probabilities underestimate the QD results for several incidence energies. However, we expect the effect on the sticking probability to be small. As Fig. 2.8d shows, most of the difference between the QD and QCT sticking probability would already disappear if the beam simulation were to be performed for cold n-H_2 (25%$j = 0$ H_2 + 75%$j = 1$ H_2). For most nozzle temperatures (incidence energies), the weight of $j = 0$ H_2 in the beam should actually be much lower than 0.25, as shown in Table 2.2, and this is especially true for $E_i > 0.2$ eV. Therefore, and because the QCT and the QD results are in good agreement for $j > 0$, the discrepancies between theory and experiment for $E_i > 0.2$ eV should not be due to using the QCT method to compute S_0.

We next turn to the limitations of the dynamical model. In our calculations with the BOSS model, we have neglected the effects of electron-hole pair excitation. However, calculations[85] on the similar H_2 + Ru(0001) system suggest that the effect of electron-hole pair excitation on the sticking coefficient should be minor. We have also neglected the effect of the surface phonons. Again, calculations[86] on H_2 sticking to Pd(110) and Pd(111) suggest that, at incidence energies > 0.2 eV where the dissociation mechanism on these surfaces becomes activated, the effect of allowing surface atom motion should become negligible. In summary, it is unlikely that the discrepancy between the present theory and the experiments of the Rendulic group is due to the use of the BOSS model in our calculations.

Finally, we come to point (iv), i.e., how PES features might have led to discrepancies between the molecular beam simulation results and the measured sticking coefficients. We first note that the two functionals that gave the best agreement with experiment (PBE-vdW2 and SRP50-vdW1) have a similar minimum barrier height and energetic corrugation. Based on the agreement with experiment we obtained with the PBE-vdW2 functional (see Fig. 2.6), we suggest that the minimum barrier height predicted by the PBE-vdW2 functional is accurate. The comparison with the results of Resch et al. at higher incidence energies suggests that the energetic corrugation of the PES may have been underestimated, assuming the results of Resch et al. to be correct. However, the theory correctly predicted the S_0 measured by Resch et al. up to about 0.3 eV. This suggests that the heights of the barriers at the bridge and hcp and fcc hollow sites computed with PBE-vdW2 may have been to small. If this

would indeed be true, the H_2 + Ni(111) system would be the first example of an H_2 + metal surface system for which the energetic corrugation of the PES is underestimated even when using a functional incorporating van der Waals correlation. For example, the PBE-vdW2 and SRP50-vdW1 functionals gave excellent results for the similar weakly activated H_2 + Ru(0001) reaction[44].

2.4 Conclusions

In this chapter we take a first step to develop a SRP-DF for H_2 on Ni(111), also investigating if the SRP-DF derived previously for H_2+Pt(111) is transferable to the system investigated. To address these questions, 6D PESs have been constructed for the dissociation of H_2+Ni(111) using nine different exchange-correlation functionals. The PESs calculated were then interpolated using the CRP method. To compare with experimentally measured sticking probabilities, quasi-classical trajectory and quantum dynamics calculations have been performed using the BOSS model.

The functionals investigated yield a wide range of barrier heights and barrier positions. The functionals containing van der Waals correlation yield barriers that are closer to the surface and exhibit a larger energetic corrugation than functionals containing PBE correlation, as previously also found for the related H_2 + Ru(0001) early barrier system.

The PBE-vdW2 and RPBE:PBE(50:50)vdW1 functionals describe the sticking experiments performed by the Rendulic group quite well, with PBE-vdW2 giving the best results. From the comparison with the most recent molecular beam experiments performed by the Rendulic group, we conclude that PBE-vdW2 can be considered to be a candidate SRP-DF for H_2 + Ni(111). However, the PBEα=0.57-vdW2 functional, which is a SRP-DF for H_2 on Pt(111) is not a SRP-DF for H_2 + Ni(111), even though Ni and Pt belong to the same group.

The PBE-vdW2 sticking probabilities are not yet in good agreement with the most recent experiments of the Rendulic group[28] for incidence energies $>$ 0.3 eV. Also, for incidence energies greater than 0.2 eV the S_0 published in an earlier paper of the Rendulic group deviated from the S_0 the group published 4 years later. For incidence energies $>$ 0.25 eV we found that S_0 starts to exhibit a considerable dependence on the beam conditions, so that some of the discrepancies noted could be due to different beam parameters characterizing the experimental beams and the beams simulated in the calculations. Other possible causes of error in the experiments have also been discussed. We consider it unlikely that the discrepancies between theory and experiment are due to using an incorrect dynamical model (BOSS) or dynamics method (QCT). In particular, except perhaps for $\nu = 0, j = 0$ initial-state resolved reaction probabilities

computed with QCT were in good agreement with QD results, so that QCT should give accurate results for sticking. However, it is possible that the PBE-vdW2 functional yields barriers for dissociation over the bridge and hollow sites that are too low. To resolve this and other questions, we advocate that new and well-defined (with respect to velocity distributions and nozzle temperatures of the beams used) experiments are performed on sticking of H_2 to Ni(111) for incidence energies > 0.2 eV.

References

(1) Chorkendorff, I.; Niemantsverdriet, J. W., *Concepts of modern catalysis and kinetics*; Wiley Online Library: 2003; Vol. 138.

(2) Ertl, G. Primary steps in catalytic synthesis of ammonia. *J. Vac. Sci. Technol., A: Vacuum, Surfaces, and Films* **1983**, *1*, 1247–1253.

(3) Noyori, R. Synthesizing our future. *Nat. Chem.* **2009**, *1*, 5–6.

(4) Díaz, C.; Pijper, E.; Olsen, R. A.; Busnengo, H. F.; Auerbach, D. J.; Kroes, G. J. Chemically accurate simulation of a prototypical surface reaction: H_2 dissociation on Cu(111). *Science* **2009**, *326*, 832–834.

(5) Kroes, G. J. Toward a database of chemically accurate barrier heights for reactions of molecules with metal surfaces. *J. Phys. Chem. Lett.* **2015**, *6*, 4106–4114.

(6) Kroes, G. J. Computational approaches to dissociative chemisorption on metals: towards chemical accuracy. *Phys. Chem. Chem. Phys.* **2021**, *23*, 8962–9048.

(7) **Tchakoua, T.**; Gerrits, N.; Smeets, E. W. F.; Kroes, G. J. SBH17: Benchmark Database of Barrier Heights for Dissociative Chemisorption on Transition Metal Surfaces. *J. Chem. Theory Comput.* **2023**, *19*, 245–270.

(8) Langreth, D. C.; Mehl, M. Beyond the local-density approximation in calculations of ground-state electronic properties. *Phys. Rev. B* **1983**, *28*, 1809.

(9) Becke, A. D. Density-functional exchange-energy approximation with correct asymptotic behavior. *Phys. Rev. A* **1988**, *38*, 3098.

(10) Perdew, J. P.; Burke, K.; Ernzerhof, M. Generalized Gradient Approximation Made Simple. *Phys. Rev. Lett.* **1996**, *77*, 3865–3868.

(11) Hammer, B. Bond activation at monatomic steps: NO dissociation at corrugated Ru(0001). *Phys. Rev. Lett.* **1999**, *83*, 3681.

(12) Peverati, R.; Truhlar, D. G. An improved and broadly accurate local approximation to the exchange–correlation density functional: The MN12-L functional for electronic structure calculations in chemistry and physics. *PCCP* **2012**, *14*, 13171–13174.

(13) Migliorini, D.; Chadwick, H.; Nattino, F.; Gutiérrez-González, A.; Dombrowski, E.; High, E. A.; Guo, H.; Utz, A. L.; Jackson, B.; Beck, R. D.; Kroes, G. J. Surface reaction barriometry: methane dissociation on flat and stepped transition-metal surfaces. *J. Phys. Chem. Lett.* **2017**, *8*, 4177–4182.

(14) Nour Ghassemi, E.; Somers, M.; Kroes, G. J. Test of the transferability of the specific reaction parameter functional for H_2+ Cu(111) to D_2+ Ag(111). *J. Phys. Chem. C* **2018**, *122*, 22939–22952.

(15) Boereboom, J.; Wijzenbroek, M.; Somers, M.; Kroes, G. Towards a specific reaction parameter density functional for reactive scattering of H_2 from Pd(111). *J. Chem. Phys.* **2013**, *139*, 244707.

(16) Ghassemi, E. N.; Somers, M. F.; Kroes, G. J. Assessment of Two Problems of Specific Reaction Parameter Density Functional Theory: Sticking and Diffraction of H_2 on Pt(111). *J. Phys. Chem. C* **2019**, *123*, 10406–10418.

(17) Kroes, G. J. Six-dimensional quantum dynamics of dissociative chemisorption of H_2 on metal surfaces. *Prog. Surf. Sci* **1999**, *60*, 1–85.

(18) Groß, A. Reactions at surfaces studied by ab initio dynamics calculations. *Surf. Sci. Rep.* **1998**, *32*, 291–340.

(19) Kroes, G. J.; Somers, M. F. Six-dimensional dynamics of dissociative chemisorption of H_2 on metal surfaces. *J. Theor. Comput. Chem.* **2005**, *4*, 493–581.

(20) Kroes, G. J.; Díaz, C. Quantum and classical dynamics of reactive scattering of H_2 from metal surfaces. *Chem. Soc. Rev.* **2016**, *45*, 3658–3700.

(21) Kroes, G. J. Frontiers in surface scattering simulations. *Science* **2008**, *321*, 794–797.

(22) Kroes, G. J. Towards chemically accurate simulation of molecule–surface reactions. *PCCP* **2012**, *14*, 14966–14981.

(23) Spiering, P.; Meyer, J. Testing Electronic Friction Models: Vibrational De-excitation in Scattering of H_2 and D_2 from Cu(111). *J. Phys. Chem. Lett.* **2018**, *9*, 1803–1808.

(24) Zhang, Y.; Maurer, R. J.; Guo, H.; Jiang, B. Hot-electron effects during reactive scattering of H_2 from Ag(111): the interplay between mode-specific electronic friction and the potential energy landscape. *Chem. Sci.* **2019**, *10*, 1089–1097.

(25) Steinrück, H.; Rendulic, K.; Winkler, A. The sticking coefficient of H_2 on Ni(111) as a function of particle energy and angle of incidence: A test of detailed balancing. *Surf. Sci.* **1985**, *154*, 99–108.

(26) Robota, H.; Vielhaber, W.; Lin, M.; Segner, J.; Ertl, G. Dynamics of interaction of H_2 and D_2 with Ni(110) and Ni(111) surfaces. *Surf. Sci.* **1985**, *155*, 101–120.

(27) Hayward, D.; Taylor, A. The variation of the sticking probability of hydrogen and deuterium on Ni(111) with energy and angle of incidence. *Chem. Phys. Lett.* **1986**, *124*, 264–267.

(28) Rendulic, K.; Anger, G.; Winkler, A. Wide range nozzle beam adsorption data for the systems H_2/nickel and H_2/Pd(100). *Surf. Sci.* **1989**, *208*, 404–424.

(29) Resch, C.; Zhukov, V.; Lugstein, A.; Berger, H.; Winkler, A.; Rendulic, K. Dynamics of hydrogen adsorption on promoter-and inhibitor-modified nickel surfaces. *Chem. Phys.* **1993**, *177*, 421–431.

(30) Hahn, C., Ph.D. Thesis, Leiden Institute of Chemistry, 2012.

(31) Bourcet, A.; Tantardini, G. F. A theoretical study of the adsorption dynamics of hydrogen on Ni(111) surface. *J. Electron. Spectrosc. Relat. Phenom.* **1994**, *69*, 55–64.

(32) Kresse, G. Dissociation and sticking of H_2 on the Ni(111), (100), and (110) substrate. *Phys. Rev. B* **2000**, *62*, 8295–8305.

(33) Perdew, J. P.; Wang, Y. Accurate and simple analytic representation of the electron-gas correlation energy. *Phys. Rev. B* **1992**, *45*, 13244.

(34) Perdew, J. P.; Chevary, J. A.; Vosko, S. H.; Jackson, K. A.; Pederson, M. R.; Singh, D. J.; Fiolhais, C. Atoms, molecules, solids, and surfaces: Applications of the generalized gradient approximation for exchange and correlation. *Phys. Rev. B* **1992**, *46*, 6671.

(35) Ghassemi, E. N.; Wijzenbroek, M.; Somers, M. F.; Kroes, G. J. Chemically accurate simulation of dissociative chemisorption of D_2 on Pt(111). *Chem. Phys. Lett.* **2017**, *683*, 329–335.

(36) Dion, M.; Rydberg, H.; Schröder, E.; Langreth, D. C.; Lundqvist, B. I. Van der Waals Density Functional for General Geometries. *Phys. Rev. Lett.* **2004**, *92*, 246401.

(37) Lee, K.; Murray, É. D.; Kong, L.; Lundqvist, B. I.; Langreth, D. C. Higher-accuracy van der Waals density functional. *Phys. Rev. B* **2010**, *82*, 081101.

(38) Madsen, G. K. H. Functional form of the generalized gradient approximation for exchange: The PBEα functional. *Phys. Rev. B* **2007**, *75*, 195108.

(39) Becke, A. D. Density-functional thermochemistry. V. Systematic optimization of exchange-correlation functionals. *J. Chem. Phys.* **1997**, *107*, 8554–8560.

(40) Hammer, B.; Hansen, L. B.; Nørskov, J. K. Improved adsorption energetics within density-functional theory using revised Perdew-Burke-Ernzerhof functionals. *Phys. Rev. B* **1999**, *59*, 7413–7421.

(41) Nattino, F.; Migliorini, D.; Kroes, G. J.; Dombrowski, E.; High, E. A.; Killelea, D. R.; Utz, A. L. Chemically accurate simulation of a polyatomic molecule-metal surface reaction. *J. Phys. Chem. Lett.* **2016**, *7*, 2402–2406.

(42) Migliorini, D.; Chadwick, H.; Kroes, G. J. Methane on a stepped surface: Dynamical insights on the dissociation of CHD_3 on Pt(111) and Pt(211). *J. Chem. Phys.* **2018**, *149*, 094701.

(43) Chadwick, H.; Migliorini, D.; Kroes, G. J. CHD_3 dissociation on Pt(111): A comparison of the reaction dynamics based on the PBE functional and on a specific reaction parameter functional. *J. Chem. Phys.* **2018**, *149*, 044701.

(44) Wijzenbroek, M.; Kroes, G. J. The effect of the exchange-correlation functional on H_2 dissociation on Ru(0001). *J. Chem. Phys.* **2014**, *140*, 084702.

(45) Wijzenbroek, M.; Klein, D. M.; Smits, B.; Somers, M. F.; Kroes, G. J. Performance of a Non-Local van der Waals Density Functional on the Dissociation of H_2 on Metal Surfaces. *J. Phys. Chem. A* **2015**, *119*, 12146–12158.

(46) Giannozzi, P. et al. Advanced capabilities for materials modelling with QUANTUM ESPRESSO. *J. Phys.: Condens. Matter* **2017**, *29*, 465901.

(47) Thonhauser, T.; Zuluaga, S.; Arter, C. A.; Berland, K.; Schröder, E.; Hyldgaard, P. Spin Signature of Nonlocal Correlation Binding in Metal-Organic Frameworks. *Phys. Rev. Lett.* **2015**, *115*, 136402.

(48) Marques, M. A.; Oliveira, M. J.; Burnus, T. Libxc: A library of exchange and correlation functionals for density functional theory. *Comput. Phys. Commun.* **2012**, *183*, 2272–2281.

(49) Blöchl, P. E. Projector augmented-wave method. *Phys. Rev. B* **1994**, *50*, 17953–17979.

(50) Dal Corso, A. Pseudopotentials periodic table: From H to Pu. *Comput. Mater. Sci.* **2014**, *95*, 337–350.

(51) Kresse, G.; Hafner, J. Ab initio molecular dynamics for liquid metals. *Phys. Rev. B* **1993**, *47*, 558–561.

(52) Kresse, G.; Hafner, J. Ab initio molecular-dynamics simulation of the liquid-metal–amorphous-semiconductor transition in germanium. *Phys. Rev. B* **1994**, *49*, 14251–14269.

(53) **Tchakoua, T**; Smeets, E. W.; Somers, M.; Kroes, G. J. Toward a Specific Reaction Parameter Density Functional for H_2+ Ni(111): Comparison of Theory with Molecular Beam Sticking Experiments. *J. Phys. Chem. C* **2019**, *123*, 20420–20433.

(54) Henkelman, G.; Jónsson, H. A dimer method for finding saddle points on high dimensional potential surfaces using only first derivatives. *J. Chem. Phys.* **1999**, *111*, 7010–7022.

(55) Heyden, A.; Bell, A. T.; Keil, F. J. Efficient methods for finding transition states in chemical reactions: Comparison of improved dimer method and partitioned rational function optimization method. *J. Chem. Phys.* **2005**, *123*, 224101.

(56) Kästner, J.; Sherwood, P. Superlinearly converging dimer method for transition state search. *J. Chem. Phys.* **2008**, *128*, 014106.

(57) Xiao, P.; Sheppard, D.; Rogal, J.; Henkelman, G. Solid-state dimer method for calculating solid-solid phase transitions. *J. Chem. Phys.* **2014**, *140*, 174104.

(58) Busnengo, H.; Salin, A.; Dong, W. Representation of the 6D potential energy surface for a diatomic molecule near a solid surface. *J. Chem. Phys.* **2000**, *112*, 7641–7651.

(59) Olsen, R. A.; Busnengo, H. F.; Salin, A.; Somers, M. F.; Kroes, G. J.; Baerends, E. J. Constructing accurate potential energy surfaces for a diatomic molecule interacting with a solid surface: H_2+ Pt(111) and H_2+ Cu(100). *J. Chem. Phys.* **2002**, *116*, 3841–3855.

(60) Karplus, M.; Porter, R. N.; Sharma, R. Exchange reactions with activation energy. I. Simple barrier potential for (H, H_2). *J. Chem. Phys.* **1965**, *43*, 3259–3287.

(61) Stoer, J.; Bulirsch, R., *Introduction to numerical analysis*; Springer Science & Business Media: 1980.

(62) Marston, C. C.; Balint-Kurti, G. G. The Fourier grid Hamiltonian method for bound state eigenvalues and eigenfunctions. *J. Chem. Phys.* **1989**, *91*, 3571–3576.

(63) Wijzenbroek, M.; Helstone, D.; Meyer, J.; Kroes, G. J. Dynamics of H_2 dissociation on the close-packed (111) surface of the noblest metal: H_2+ Au(111). *J. Chem. Phys.* **2016**, *145*, 144701.

(64) Kosloff, R. Time-dependent quantum-mechanical methods for molecular dynamics. *J. Phys. Chem.* **1988**, *92*, 2087–2100.

(65) Kosloff, D.; Kosloff, R. A Fourier method solution for the time dependent Schrödinger equation as a tool in molecular dynamics. *J. Comput. Phys.* **1983**, *52*, 35–53.

(66) Corey, G. C.; Lemoine, D. Pseudospectral method for solving the time-dependent Schrödinger equation in spherical coordinates. *J. Chem. Phys.* **1992**, *97*, 4115–4126.

(67) Lemoine, D. The finite basis representation as the primary space in multidimensional pseudospectral schemes. *J. Chem. Phys.* **1994**, *101*, 10526–10532.

(68) Feit, M.; Fleck Jr, J.; Steiger, A. Solution of the Schrödinger equation by a spectral method. *J. Comput. Phys.* **1982**, *47*, 412–433.

(69) Balint-Kurti, G. G.; Dixon, R. N.; Marston, C. C. Time-dependent quantum dynamics of molecular photofragmentation processes. *J. Chem. Soc., Faraday Trans.* **1990**, *86*, 1741–1749.

(70) Balint-Kurti, G. G.; Dixon, R. N.; Marston, C. C. Grid methods for solving the Schrödinger equation and time dependent quantum dynamics of molecular photofragmentation and reactive scattering processes. *Int. Rev. Phys. Chem.* **1992**, *11*, 317–344.

(71) Mowrey, R. C.; Kroes, G. J. Application of an efficient asymptotic analysis method to molecule–surface scattering. *J. Chem. Phys.* **1995**, *103*, 1216–1225.

(72) Vibok, A.; Balint-Kurti, G. Parametrization of complex absorbing potentials for time-dependent quantum dynamics. *J. Phys. Chem.* **1992**, *96*, 8712–8719.

(73) Pijper, E.; Kroes, G. J.; Olsen, R. A.; Baerends, E. J. Reactive and diffractive scattering of H_2 from Pt(111) studied using a six-dimensional wave packet method. *J. Chem. Phys.* **2002**, *117*, 5885–5898.

(74) Rettner, C.; Michelsen, H.; Auerbach, D. Quantum-state-specific dynamics of the dissociative adsorption and associative desorption of H_2 at a Cu(111) surface. *J. Chem. Phys.* **1995**, *102*, 4625–4641.

(75) Gallagher, R. J.; Fenn, J. B. Relaxation rates from time of flight analysis of molecular beams. *J. Chem. Phys.* **1974**, *60*, 3487–3491.

(76) Díaz, C.; Olsen, R. A.; Auerbach, D. J.; Kroes, G. J. Six-dimensional dynamics study of reactive and non reactive scattering of H_2 from Cu(111) using a chemically accurate potential energy surface. *Phys. Chem. Chem. Phys.* **2010**, *12*, 6499–6519.

(77) Michelsen, H. A.; Auerbach, D. J. A critical examination of data on the dissociative adsorption and associative desorption of hydrogen at copper surfaces. *J. Chem. Phys.* **1991**, *94*, 7502–7520.

(78) Berger, H. F., Ph.D. Thesis, Technische Universitat Graz, 1992.

(79) Marquardt, D. W. An Algorithm for Least-Squares Estimation of Nonlinear Parameters. *J. Soc. Ind. Appl. Math.* **1963**, *11*, 431–441.

(80) Perdew, J. P.; Schmidt, K. Jacob's ladder of density functional approximations for the exchange-correlation energy. *AIP Conf. Proc.* **2001**, *577*, 1–20.

(81) Gross, A.; Hammer, B.; Scheffler, M.; Brenig, W. High-dimensional quantum dynamics of adsorption and desorption of H_2 at Cu(111). *Phys. Rev. Lett.* **1994**, *73*, 3121.

(82) Ghassemi, E. N.; Smeets, E. W. F.; Somers, M. F.; Kroes, G. J.; Groot, I. M.; Juurlink, L. B.; Füchsel, G. Transferability of the specific reaction parameter density functional for H_2 + Pt(111) to H_2 + Pt(211). *J. Phys. Chem. C* **2019**, *123*, 2973–2986.

(83) Smeets, E. W. F.; Voss, J.; Kroes, G. J. Specific Reaction Parameter Density Functional Based on the Meta-Generalized Gradient Approximation: Application to H_2+Cu(111) and H_2+Ag(111). *J. Phys. Chem. A* **2019**, *123*, 5395–5406.

(84) Chen, J.-C.; Juanes-Marcos, J. C.; Woittequand, S.; Somers, M. F.; Díaz, C.; Olsen, R. A.; Kroes, G. J. Six-dimensional quasiclassical and quantum dynamics of H_2 dissociation on the c (2× 2)-Ti/Al(100) surface. *J. Chem. Phys.* **2011**, *134*, 114708.

(85) Füchsel, G.; Schimka, S.; Saalfrank, P. On the role of electronic friction for dissociative adsorption and scattering of hydrogen molecules at a Ru(0001) surface. *J. Phys. Chem. A* **2013**, *117*, 8761–8769.

(86) Busnengo, H.; Di Césare, M.; Dong, W.; Salin, A. Surface temperature effects in dynamic trapping mediated adsorption of light molecules on metal surfaces: H_2 on Pd (111) and Pd (110). *Phys. Rev. B* **2005**, *72*, 125411.